Journal of Power Sources 185 (2008) 641–648

Contents lists available at ScienceDirect

Journal of Power Sources

journal homepage: www.elsevier.com/locate/jpowsour

Characterization and optimization of $La_{0.8}Sr_{0.2}Sc_{0.1}Mn_{0.9}O_{3-\delta}$-based composite electrodes for intermediate-temperature solid-oxide fuel cells

Yao Zheng, Ran Ran, Hongxia Gu, Rui Cai, Zongping Shao *

State Key Laboratory of Materials-Oriented Chemical Engineering, College of Chemistry & Chemical Engineering, Nanjing University of Technology, No. 5 Xin Mofan Road, Nanjing 210009, PR China

ARTICLE INFO

Article history:
Received 22 July 2008
Received in revised form 30 August 2008
Accepted 1 September 2008
Available online 7 September 2008

Keywords:
Intermediate-temperature solid-oxide fuel cells
$La_{0.8}Sr_{0.2}Sc_{0.1}Mn_{0.9}O_{3-\delta}$
Composite cathodes
Electrochemical impedance spectroscopy
Oxygen reduction

ABSTRACT

Composite electrodes composed of a perovskite-type $La_{0.8}Sr_{0.2}Sc_{0.1}Mn_{0.9}O_{3-\delta}$ (LSSM) and a fluorite-type scandium-stabilized zirconia (ScSZ) were prepared and evaluated as potential cathodes for intermediate-temperature solid-oxide fuel cells. Characterization was made by phase reaction, electrochemical impedance spectroscopy, step current polarization and *I–V* tests. The phase reaction between LSSM and ScSZ occurred at 1150 °C or higher; however, it had a minor effect on the electrode performance. The formation of a composite electrode led to an obvious improvement in both charge transfer and surface-related processes. With the increase of ScSZ content, the rate-limiting step of oxygen reduction reaction steadily changed from mainly a surface diffusion process to an electron transfer process. The optimal ScSZ content and sintering temperature of the electrode layer were found to be 20 wt.% and 1100–1150 °C, respectively. Under optimal conditions, an anode-supported single cell with LSSM + ScSZ composite cathode showed high power densities of ~1211 and 386 mW cm^{-2} at 800 and 650 °C, respectively.

1. Introduction

The solid-oxide fuel cell (SOFC) is an all-solid electrochemical device which converts chemical energy to electrical power at elevated temperature with very high efficiency and low emissions. A single SOFC is composed of a porous anode and a porous cathode, separated by a dense electrolyte. The single cells are stacked in series or/and parallel to meet the potential and power requirements for practical application. A typical SOFC is composed of an yttria-stabilized zirconia electrolyte and lanthanum strontium manganese (LSM) cathode operated at around 1000 °C. Nowadays, it has been well recognized that multiple benefits can be derived by reducing the operating temperature of a SOFC to the intermediate temperature range of 500–800 °C, including reduced fabrication cost, prolonged life time, versatile cell materials, and elegant sealing [1–7].

Cathode is the location at which oxygen reduction reaction takes place. Since oxygen activation is normally much more difficult than that of hydrogen, with the drop of operating temperature, the polarization resistance for a SOFC with thin-film electrolyte originates primarily from the cathode [8–10]. The development of a cathode with high electrocatalytic activity for oxygen reduction is thereby critical for the production of intermediate-temperature (IT)-SOFCs. It is well known that cathode performance is determined by many factors, such as electrical conductivity, the thermal expansion coefficient, phase reactions between the electrolyte and electrode, and oxygen surface exchange and bulk diffusion properties of the cathode material [2,8]. A synergetic effect between electrolyte and electrode may also be observed. For example, a mixed conducting perovskite-type $Ba_{0.5}Sr_{0.5}Co_{0.8}Fe_{0.2}O_{3-\delta}$ oxide that performs well on a doped ceria electrolyte did not perform as well on stabilized zirconia electrolytes [5,11–13]. Thus, the electrode material and microstructure should be specially tailored for the individual electrolyte.

Stabilized zirconia is still the most commonly used electrolyte in SOFC due to its excellent mechanical properties, favorable redox stability, and negligible electronic conductivity. Scandia-stabilized zirconia (ScSZ) shows the highest ionic conductivity among the lanthanide-stabilized zirconias and has received considerable attention recently [14–17]. Today, the typical cathode material matching the ScSZ electrolyte is still the LSM oxide, although it shows poor activity for oxygen reduction at reduced temperatures. Many strategies have been exploited to improve its cathodic performance at reduced temperature, such as optimizing the microstructure of the cathode and electrolyte interface [18–20], surface modification of the LSM with precious metals such as Ag or Pt [21–24] or samaria or gadolinia doped ceria [25,26], or polarizing under direct cathodic current for a limited period of time

* Corresponding author. Tel.: +86 25 83587722; fax: +86 25 83365813.
E-mail address: shaozp@njut.edu.cn (Z. Shao).

0378-7753/$ – see front matter © 2008 Elsevier B.V. All rights reserved.
doi:10.1016/j.jpowsour.2008.09.003

to create oxygen vacancies on the surface or inside the bulk of the LSM [27–29]. The simplest and most widely applied technique still involves introducing an ionic conducting phase such as YSZ and ScSZ into the LSM to form a composite electrode [30–39]. It is believed that the improvement in cathode performance by the formation of composite electrode is due to the extension of active sites from the typical electrolyte–electrode–air triple-phase boundary (TPB) into the electrode bulk. Furthermore, the thermal expansion compatibility and adhesion of the electrode to electrolyte is also improved.

Recently, we demonstrated that doping a proper amount of Sc^{3+} into the B-site of LSM perovskite with the formation of $La_{0.8}Sr_{0.2}Sc_yMn_{1-y}O_{3-\delta}$ ($y = 0.0$–0.2) solid solution resulted in an improved cathode performance for the facilitation of the creation of oxygen vacancies inside the oxide bulk under current polarization [40]. In this study, to further improve the cathode performance of the $La_{0.8}Sr_{0.2}Sc_{0.1}Mn_{0.9}O_{3-\delta}$ (LSSM) oxide at intermediate temperatures, composite electrodes were synthesized and evaluated as cathodes on a ScSZ electrolyte, adopting ScSZ as a second phase. The optimal LSSM to ScSZ ratio and the fabrication parameters were determined.

2. Experimental

2.1. Material synthesis and characterization

Both LSSM and ScSZ oxide powders were synthesized via an EDTA–citrate complexing sol–gel process [41] with $La(NO_3)_3{\cdot}xH_2O$, $Sr(NO_3)_2$, $Mn(CH_3COO)_2{\cdot}4H_2O$, $Zr(NO_3)_4{\cdot}5H_2O$ and Sc_2O_3 (all in A.R. grade) as the raw materials for the cation sources. Sc_2O_3 powder was prepared in an aqueous solution by dissolving it in diluted nitric acid with heating and magnetic stirring before applying the sol–gel synthesis. The preparation of LSSM, for example, is described as follows. The required amounts of metal nitrates and $Mn(CH_3COO)_2{\cdot}4H_2O$, according to the nominal molecular composition of the target product, were prepared in an aqueous solution. EDTA and citric acid, both acted as complexing agents, were added to the solution in sequence. The pH of the solution was adjusted to ~6 via the addition of $NH_3{\cdot}H_2O$. After evaporating the water from the mixture via heating, a transparent gel was obtained. It was pre-fired at 250 °C forming a solid precursor, which was subsequently calcinated at 1000 °C for 5 h under an air atmosphere to yield the desired product. The phase structures of the oxide materials were investigated by X-ray diffraction using a Bruker D8 Advance Diffractormeter. Diffraction patterns were collected at room temperature by step scanning angles (2θ) between 20° and 80°.

2.2. Electrochemical characterization

Electrochemical characterization of the composite electrodes with ScSZ content varying from 0 to 50 wt.% was conducted using a three-electrode electrochemical cell [40]. Electrolyte disks were prepared from $(Sc_2O_3)_{0.1}(ZrO_2)_{0.9}$ (ScSZ) powder by die pressing and were sintered at 1500 °C for 5 h under an air atmosphere. The thickness and diameter of a sintered disk were 0.3 and 16 mm, respectively. Isopropyl alcohol-based slurry containing LSSM and the proper amount of ScSZ was sprayed on one side of the electrolyte substrate and then calcinated at 1000–1200 °C in air for 2 h to form the working electrode. Ethanol-based silver slurry was applied to the other side of the electrolyte as symmetrically as possible with the working electrode acting as the counter electrode. Silver paste (DAD-87, Shanghai, China) was used as the reference electrode and was painted in a ring surrounding the counter electrode. The gap between the counter electrode and reference electrode was ~4 mm, and the area of the working electrode, counter electrode and reference electrode was 0.26, 0.26 and 0.3 cm^2, respectively.

The cathodic polarization resistance was measured using a Solartron 1260A frequency response analyzer in combination with a Solartron 1287 potentiostat/galvonostat. The frequency range of the electrochemical impedance spectroscopy (EIS) measurement was from 0.1 Hz to 1000 kHz, and the signal amplitude was 10 mV. Data were collected using Zplot 2.9c software. The polarization current was varied from 0 to 1000 mA cm^{-2} in 10 mA intervals. The results were applied to correct for the IR drop corresponding to the electrolyte and lead resistances, thereby establishing resistance-free I/E characteristics. Series resistance data obtained from EIS measurements were used to make this correction. The overall impedance data were fit by a complex non-linear least square (CNLS) fitting program by Z-View 2.9c software.

2.3. Single-cell test

Anode-supported cells were adopted for a performance evaluation of the composite electrodes under actual fuel cell conditions. The anode was made from NiO and ScSZ mixture with a weight ratio of 60 to 40. An electrolyte membrane was fabricated onto NiO + ScSZ substrate using a dual-dry pressing followed by co-firing at 1500 °C in air for 5 h. A slurry, prepared by dispersing composite cathode powder into an isopropyl alcohol liquid medium, was sprayed on the electrolyte surface, which was subsequently calcinated at 1100–1150 °C in air for 2 h. Silver paste was adopted as a current collector. Fuel cell performance was assessed via I–V characterization at temperatures between 650 and 800 °C. Measurements were performed using a digital sourcemeter (Keithely 2420) which was interfaced with a computer to facilitate data acquisition.

3. Results and discussion

3.1. Reactivity between LSSM and ScSZ

When LSSM and ScSZ composite oxides are applied as the electrodes for a ScSZ-electrolyte SOFC, the phase reaction between LSSM and ScSZ may happen both inside the composite electrodes and also at the electrode–electrolyte interfaces. Such a reaction is likely at high operating temperature or during the firing of the electrode layer onto the electrolyte surface. It has been demonstrated that the phase reaction between a LSM electrode and YSZ electrolyte has happened at high temperatures and led to the formation of a $La_2Zr_2O_7$ insulating phase, which could block the ionic diffusion and led to a substantial increase of interfacial polarization resistance [42]. To systematically investigate the phase reaction, LSSM and ScSZ powders in a 50:50 weight ratio were well mixed by grinding with an agate mortar and pestle. The resultant mixed powders were then calcinated at various temperatures under an air atmosphere for 2 h. After cooling down to room temperature naturally, the powders underwent a phase composition analysis. As shown in Fig. 1, all the diffraction patterns of the powders can be indexed based on the physical mixture of LSSM and ScSZ oxides when the calcination temperature was 1000, 1050 or 1100 °C. This suggests that the solid-phase reaction between LSSM and ScSZ was negligible under such circumstances. With the further increase of calcination temperature to 1150 °C, the characteristic diffraction peak of a pyrochlore-type $La_2Zr_2O_7$ at $2\theta = 28.3°$ started to appear, although weak in intensity, and the peak intensity was strengthened with the further increase of firing temperature. The reaction

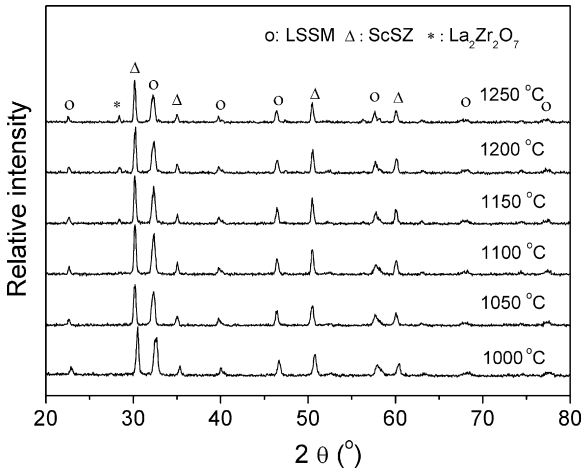

Fig. 1. X-ray diffraction patterns of LSSM and ScSZ (50:50 wt.%) composite after sintered at various temperatures for 2 h in air.

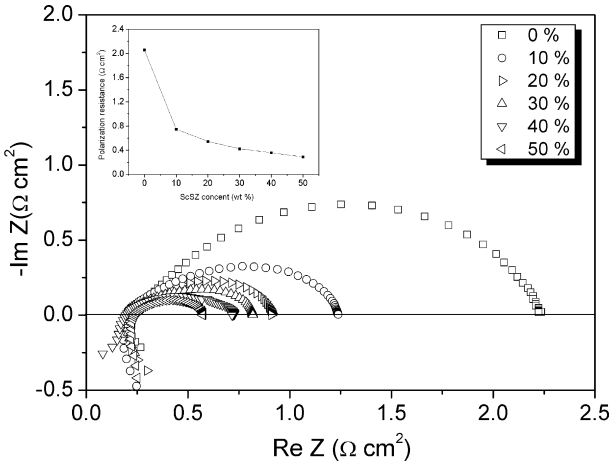

Fig. 2. EIS of ScSZ + LSSM electrodes with various ScSZ contents at 800 °C, measured under zero direct current passage.

can be described by the following equation:

$$La_{0.8}Sr_{0.2}Sc_{0.1}Mn_{0.9}O_3 + (Sc_2O_3)_{0.1}(ZrO_2)_{0.9} \rightarrow La_{0.8-x}Sr_{0.2}Sc_{0.1}Mn_{0.9}O_{3-3x/2} + (x/2)La_2Zr_2O_7 + (Sc_2O_3)_{0.1}(ZrO_2)_{0.9-x} \quad (1)$$

Since $La_2Zr_2O_7$ is an insulating phase, the phase reaction between LSSM and ScSZ may have an impact on the electrode performance, which will be discussed in detail later.

3.2. Effect of ScSZ to LSSM ratio on the electrode performance

A composite electrode has been widely applied to improve the performance of LSM-based material for oxygen reduction at intermediate temperatures. It was reported that the best activity for oxygen reduction of a LSM + YSZ composite electrode was achieved at a YSZ content of 20–40 wt.% [32,36,38]. The effect of ScSZ on the performance of a LSSM + ScSZ composite electrode for oxygen reduction, and the optimal ScSZ weight content was investigated by EIS and step current polarization (SCP) based on a three-electrode configuration. To avoid the impact of phase reaction on the electrode performance, a sintering temperature of 1100 °C was adopted for this study.

The EIS of LSSM + ScSZ composite electrodes with various ScSZ contents at an operating temperature of 800 °C, measured under an air atmosphere and zero direct current passage are shown in Fig. 2. For the pure LSSM electrode, the area specific polarization resistance (ASR) reached 2.1 Ω cm^2, which is only slightly improved as compared to the typical value for a LSM electrode [8–10,30,32,38]. We have demonstrated previously that partial substitution of Mn^{4+} in LSM by Sc^{3+} did not introduce ionic conductivity into the oxide under zero direct current passage, i.e., the oxygen reduction over the LSSM electrode was still strictly limited to the TPB region. However, introducing ScSZ as a second phase with a content as low as 10 wt.% substantially reduced the ASR to a value of ~0.75 Ω cm^2 at 800 °C. With the further increase of ScSZ content, the ASR decreased steadily. It reached ~0.39 Ω cm^2 at a ScSZ content of 50 wt.%. It is clear that the introduction of the ScSZ phase effectively increased the electrode activity for oxygen reduction.

The overall electrochemical reaction for oxygen reduction over the cathode of an SOFC can be described as follows:

$$O_2(g) + 4e^- = 2O^{2-} \quad (2)$$

In reality, it may involve many sub-steps, such as oxygen gas diffusion, oxygen surface adsorption, oxygen dissociation, electron transfer, oxygen-ion transfer, etc. To determine the role of the ScSZ phase in the composite electrode on oxygen reduction, the EIS data were fit to an equivalent circuit composed of two R/CPE units in series with an electrolytic resistor (R_0) and an inductor (L_0). A constant phase element (CPE) represents a non-ideal capacitor of the double layer at a non-planar TPB. The high-frequency arc is typically associated with the transport/transfer of oxygen intermediates/oxide ions between electrode and electrolyte and through the composite electrode. The intermediate-frequency arc is related with the surface diffusion process, which may include the oxygen surface adsorption, oxygen dissociation, oxygen (oxygen-ion) surface diffusion, and electron transfer [8,30–32,43–45]. A typical fitting result is shown in Fig. 3a with the equivalent circuit presented as an insert. The effect of the ScSZ content in the composite electrode on the size of the high-frequency arc and intermediate-frequency arc are presented in Fig. 3b. The size of both arcs decreased significantly and monotonically with the increase of ScSZ content, implying both processes were improved after the introduction of the ScSZ phase. The improvement in the oxygen-ion charge transfer process (high-frequency arc) with the increase of ScSZ content can be explained by the increased nominal ionic conductivity, while the increase in surface diffusion activity was attributed to the improved oxygen surface diffusion and oxygen dissociation processes. Both are facilitated by the increase of surface oxygen vacancy. Since oxygen surface reaction (dissociation and incorporation) on stabilized zirconia is known to be slow, only the diffusion process is likely to be significant; therefore the sizes of intermediate-frequency arcs decreased more significantly than high-frequency ones, as shown in Fig. 3b.

It is well known that LSM can be partially reduced under a cathodic polarization, which leads to a substantial increase of its activity for oxygen reduction due to the formation of a large number of re-generated oxygen vacancies [27–29,39,46]. Thus, we here investigated the behavior of LSSM + ScSZ composite electrodes under a cathodic polarization. Fig. 4 shows the impedance spectroscopes of the corresponding LSSM + ScSZ electrodes in Fig. 2 after a cathodic polarization at −0.5 V for 40 min. An additional depressed semicircle appeared at the low-frequency range (several Hz). A similar appearance of a low-frequency arc was also observed in the literature for a typical LSM electrode after its polarization [30,38], where this was attributed to the non-charge-related gas phase oxygen diffusion process. Since gas phase diffusion is not

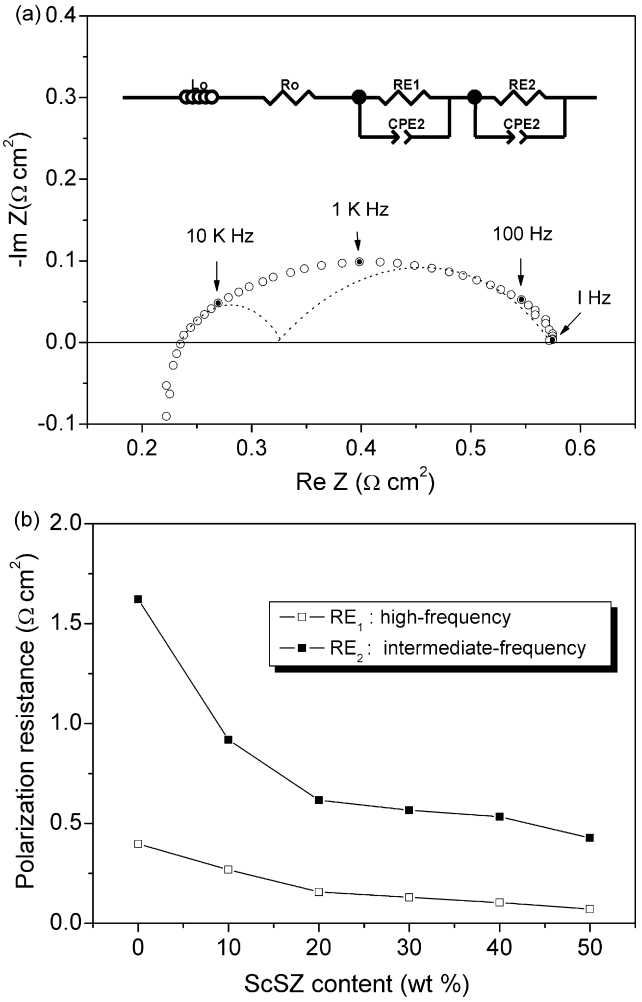

Fig. 3. (a) A typical fitting result of EIS of 50 wt.% ScSZ electrodes before cathodic polarization and (b) the polarization resistance for the high-frequency and intermediate-frequency arcs of the data in Fig. 2 via the equivalent circuit as shown in (a).

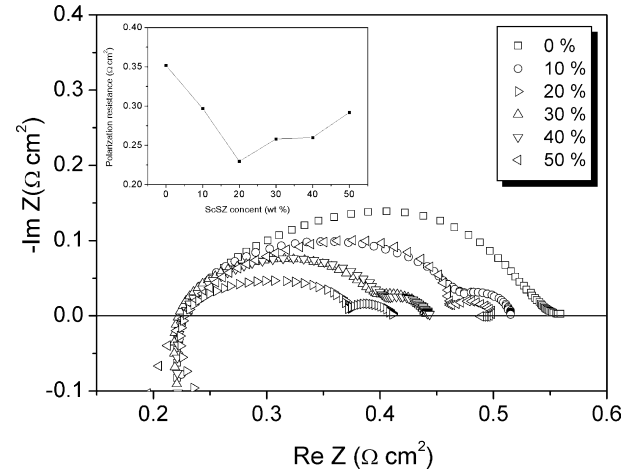

Fig. 4. EIS of ScSZ + LSSM electrodes with various ScSZ contents at 800 °C, measured after a cathodic polarization at −0.5 V for 40 min.

an intrinsic property of an electrode, only the semicircle at the high to intermediate-frequency range was considered for further analysis. Overall, the increase in ScSZ content first resulted in a decrease in overall polarization resistance. It reached a minimum value of ~0.22 Ω cm² at a ScSZ content of 20 wt.% at 800 °C (the gas phase diffusion polarization resistance was not included), and then increased with the further increase of ScSZ content. Such a trend is different from that before the polarization, which showed a steady decrease in polarization resistance with the increase of ScSZ content. If we compare the corresponding ASRs for the composite electrodes before and after the polarization, it was found that all the samples showed an improvement in polarization resistance for oxygen reduction after the cathodic polarization, however, the higher the ScSZ content the less the improvement in overall polarization resistance was observed.

Under polarization, the Mn^{4+} in LSSM lattice was partially reduced and led to the formation of oxygen vacancy both over the surface and inside the oxide bulk, which then effectively improved the surface exchange kinetics due to the increased number of active sites for oxygen reduction. The EIS in Fig. 4 was also fit to an equivalent circuit by modifying the existing one as shown in Fig. 3a by adding a new R/CPE (R_3/CPE_3) unit in series to simulate the gas phase diffusion process of the low-frequency arc. Fig. 5a shows a typical result with the equivalent circuit presented as an insert. The

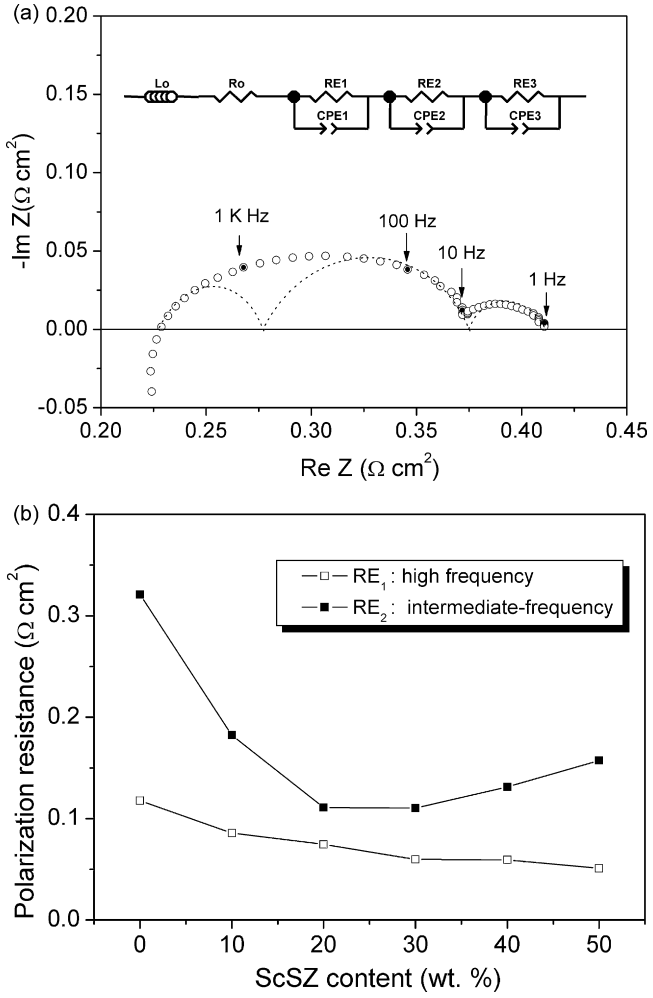

Fig. 5. (a) A typical fitting result of EIS of 20 wt.% ScSZ electrodes after a cathodic polarization at −0.5 V for 40 min and (b) the polarization resistance for the high-frequency and intermediate-frequency arcs of the data in Fig. 4 via the equivalent circuit as shown in Fig. 5a.

derived high-frequency arc was associated with the ion transport process, while the intermediate-frequency arc was related to the surface diffusion, oxygen dissociation, and electron transport processes. As compared to that before polarization (Fig. 3b), the ASR of the ion transport process after the polarization was reduced for all the samples with various ScSZ contents (Fig. 5b), agreed well with the increased nominal ionic conductivity contributed from the LSSM phase because of the partial reduction. Similar to that before polarization, the polarization resistance of the ion transport process decreased monotonically with the increase of ScSZ content. As to the intermediate-frequency arc, the size first decreased with ScSZ content, reached a minimum value at a ScSZ content of 20 wt.%, then remained almost constant with an increase of ScSZ content to 30 wt.%, and then increased sharply with the further increase of ScSZ content to 40 wt.% and higher (Fig. 5b). Such a phenomenon can be explained as follows. Under polarization, the LSSM is partially reduced, increasing the surface oxygen vacancy concentration on the one hand, which is beneficial for improving the oxygen dissociation and oxygen surface diffusion; on the other hand, the creation of oxygen vacancy results in a decrease in electrical conductivity, detrimental to the electron charge transfer process. The increase of the polarization resistance for the surface diffusion process at a ScSZ content of >20 wt.% suggests the electronic charge transfer became predominant in the rate determination in the surface diffusion processes.

To further demonstrate the effect of ScSZ on the oxygen reduction process in the composite electrode, the dependence of $1/R$ versus the inverse oxygen partial pressure of the atmosphere $1/P_{O_2}$ was conducted, where the polarization resistance R was a sum of R_{E1} and R_{E2} in Fig. 5a. The slope (n) has significant information on the oxygen reduction process [32,43–45]. Fig. 6 shows the dependence of n on ScSZ content in the LSSM + ScSZ composite electrode at 800 °C within the oxygen partial pressure range from 0.002–1.0 atm. It decreased steadily with the increase of ScSZ content, from an initial value of ~0.56 at 0 wt.% ScSZ (pure LSSM) to a value of ~0.30 with 50 wt.% ScSZ. Typically, a value of 0.5 for n is an indication of the rate-limiting by oxygen surface diffusion or oxygen dissociation while 1/4 should be observed for an electron charge transfer process. It then suggests that the rate-limiting step for the oxygen reduction process changes steadily from mainly a surface diffusion process to an electron transfer process ($n = 0.25$).

Table 1 shows the activation energy (E_a) of the impedance polarization with respect to the temperature at various ScSZ contents before and after the polarization. All the E_a are between 110 and 150 kJ mol^{-1}, similar to the literature results for a LSM cathode [8–10,30,32,38]. The lowest E_a was also achieved at a ScSZ content of 20 wt.%.

Table 1
Activation energy (E_a) of the impedance polarization with respect to the temperature at various ScSZ contents before and after the polarization.

	Activation energy (kJ mol^{-1})					
	ScSZ content (%)					
	0	10	20	30	40	50
Before polarization	146.24	132.29	127.57	123.70	120.26	114.70
After polarization	130.56	126.30	111.28	116.05	126.70	118.54

The performance of LSSM + ScSZ composite electrodes was further investigated by the step current polarization experiment. Fig. 7 shows the overpotential–current curves of LSSM + ScSZ electrodes with various ScSZ contents at 800 °C. At low current density, for example −0.1 A cm^{-1}, the overpotential has the sequence of LSSM > LSSM–10% ScSZ > LSSM–40% ScSZ ~ LSSM–50% ScSZ > LSSM–30% ScSZ ~ LSSM–20% ScSZ. At a higher current density of −1 A cm^{-1}, the sequence changed to LSSM > LSSM–10% ScSZ > LSSM–50% ScSZ > LSSM–40% ScSZ > LSSM–30% ScSZ > LSSM–20% ScSZ. This further supports the idea that the optimal ScSZ content for a LSSM + ScSZ composite electrode is around 20 wt.%.

3.3. Effect of sintering temperature on the electrode performance

For practical application, the electrode should be fabricated onto the electrolyte surface. To determine the best sintering temperature for the electrode layer, the LSSM + ScSZ composite electrode with the ScSZ content of 20 wt.% was fabricated onto the ScSZ electrolyte surface at various firing temperatures. Fig. 8a and b shows the ASRs of the corresponding electrodes before and after polarization at −0.5 V at 800 °C for 40 min, respectively. The increase of sintering temperature first resulted in a decrease in polarization resistance up to 1100 °C, both before and after the polarization. A slight increase of the ASR was observed when the temperature increased to 1150 °C. The further increase in sintering temperature, however, resulted in a sharp increase in the polarization resistance. Therefore, the optimal sintering temperature for the electrode layer should be between 1000 and 1150 °C.

As demonstrated previously, sintering is required for adhesion of electrode and electrolyte, but high-temperature calcination could result in a phase reaction between LSSM and ScSZ both

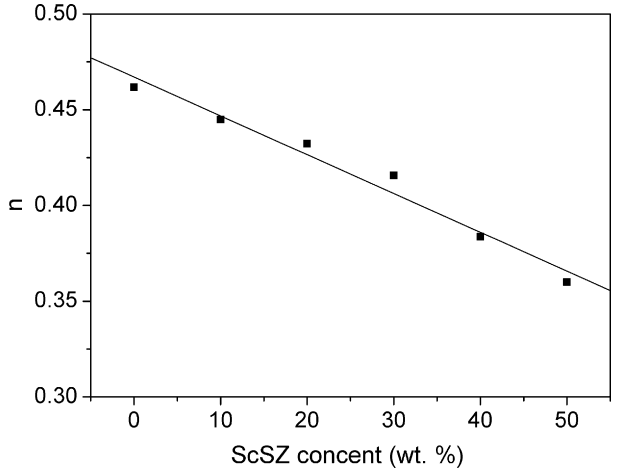

Fig. 6. The dependence of n on the ScSZ content in the composite oxide at 800 °C.

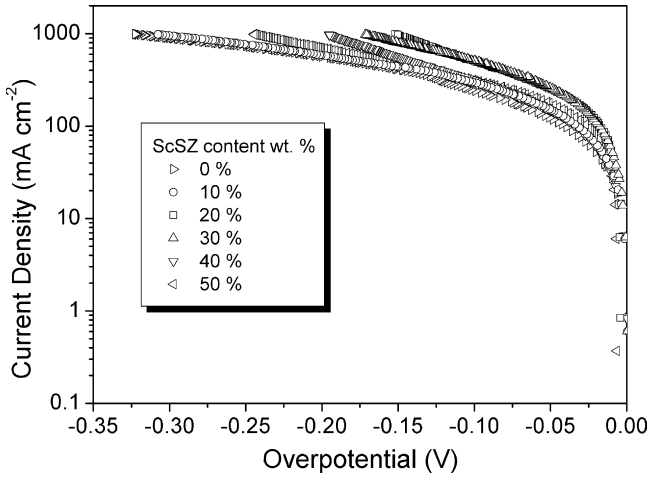

Fig. 7. The overpotential–current curves of LSSM + ScSZ electrode with various ScSZ contents at 800 °C.

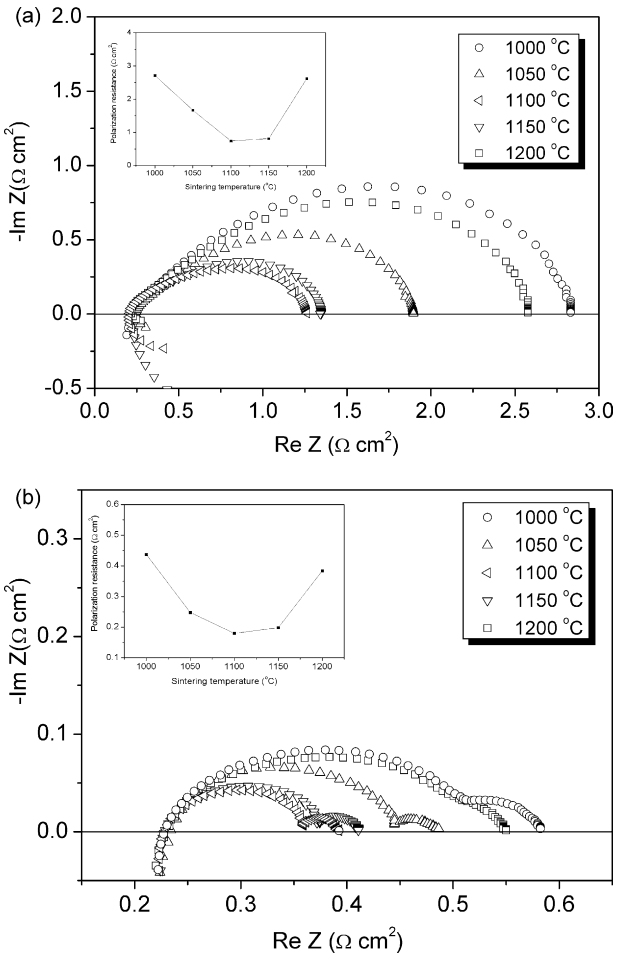

Fig. 8. (a) The ASRs of composite electrodes sintered at various temperatures before polarization and (b) the ASRs of composite electrodes sintered at various temperatures after polarized at −0.5 V for 40 min.

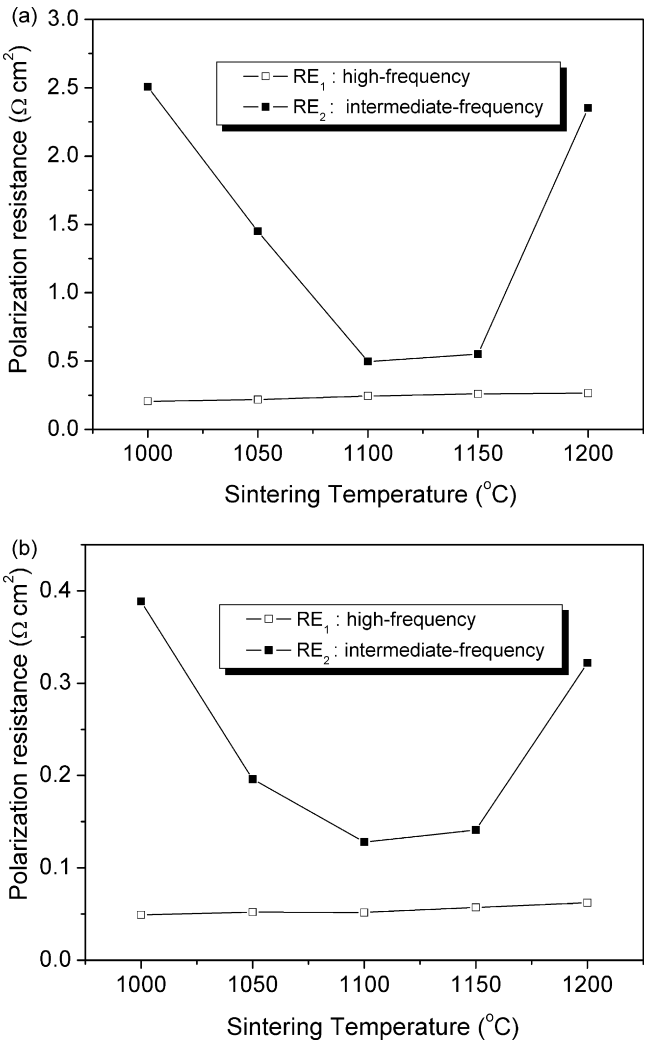

Fig. 9. (a) The fitting values of Fig. 8a by the model in Fig. 3a and (b) the fitting values of Fig. 8b by the model in Fig. 5a.

inside the electrode and between the electrode and electrolyte layer with the formation of $La_2Zr_2O_7$. Since $La_2Zr_2O_7$ is an insulating phase with negligible ionic and electronic conductivity, it will block the oxygen-ion transfer through the electrode–electrolyte interface, resulting in an increase of interfacial polarization resistance when located between the LSSM and electrolyte interface. On the other hand, a certain degree of solid-phase reaction between the electrode and electrolyte layers is helpful for reducing the contact resistance by increasing the connection between the electrode particles and between the electrode and the electrolyte layer. Furthermore, a slight A-site deficiency in perovskite created via reaction (1) at high calcination temperature is also beneficial for oxygen reduction since it may introduce oxygen vacancies into the oxide bulk [46–48]. Fig. 9a and b is ASRs of the high frequency and intermediate arcs before and after the cathodic polarization. A steady increase in the size of high-frequency arc supported the fact that the solid-phase reaction between LSSM and ScSZ became more serious with the increase of firing temperature. The size of the high-frequency arc was, however, still much smaller than the intermediate-frequency arc, suggesting the polarization resistance of the oxygen ionic charge transfer was relatively small as compared to that of surface diffusion/electron charge transfer processes. This implies that the solid-phase reaction between LSSM and ScSZ at high temperature did not have significant effect on the oxygen reduction over a LSSM + ScSZ composite electrode. The polarization resistance for the intermediate-frequency arc first envisaged a decrease with sintering temperature, reached a minimum at a sintering temperature between 1100 and 1150 °C, and then increased obviously with the further increase of temperature. Such a phenomenon could be explained as follows. The increase in firing temperature resulted in a better contact between LSSM and ScSZ, which was beneficial for reducing the interfacial diffusion resistance. On the other hand, it also resulted in a decrease of the absolute electrode surface area, which was detrimental to the oxygen surface reduction. Calcination at 1100–1150 °C resulted in a sound connection between LSSM and ScSZ in the electrode and also a favorable electrode surface area.

Table 2 contains the activation energies calculated based on the temperature dependence of the polarization resistance before and after the polarization. The measured values were also within the

Table 2
Activation energy (E_a) of the impedance polarization with respect to the temperature at various sintering temperatures before and after the polarization.

	Activation energy (kJ mol^{-1})				
	Sintering temperature (°C)				
	1000	1050	1100	1150	1200
Before polarization	143.31	135.24	127.57	131.01	146.51
After polarization	139.55	135.71	111.28	124.68	144.58

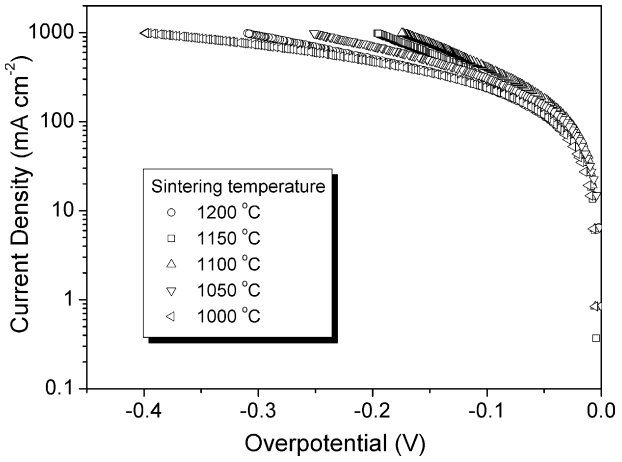

Fig. 10. The overpotential–current curves of the LSSM + ScSZ electrodes sintered at various temperatures testing at 800 °C.

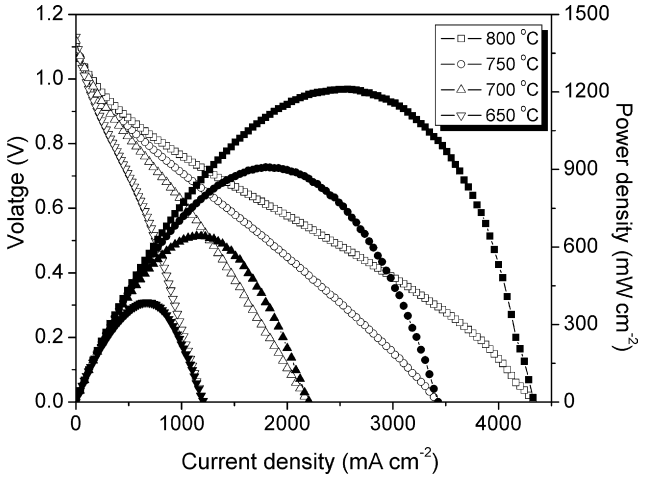

Fig. 12. The *I–V* and *I–P* curves of single cell with 80 wt.% LSSM + 20 wt.% ScSZ cathode at various temperatures.

range of 110–150 kJ mol^{-1}, similar to the literature results for typical LSM + YSZ electrodes. The electrode fired at 1100 °C showed the lowest activation energy both before and after the polarization, followed by the 1150 °C fired one. This further implies that the best sintering temperature for the cathode layer is 1100–1150 °C. The optimal sintering temperature was further determined by the step current polarization of an 80 wt.% LSSM + 20 wt.% ScSZ composite electrode. Fig. 10 shows the overpotential–current curves of the LSSM + ScSZ electrodes fired at various temperatures for 2 h. The electrode fired at 1100 °C showed the lowest overpotential, followed by the one fired at 1150, 1050, 1200 and 1000 °C.

3.4. Single-cell performance

To demonstrate the performance of LSSM + ScSZ composite electrodes in complete cells under real fuel cell conditions, ScSZ + Ni supported thin-film (~25 μm) ScSZ electrolyte fuel cells with LSSM + ScSZ cathodes were fabricated. The cathode layers were put onto the electrolyte surfaces at the optimal firing temperature of 1100–1150 °C. The ScSZ content of 0–40 wt.% in the composite electrodes was investigated. Fig. 11 shows the *I–V* and *I–P* curves of the cells sintered at 1150 °C for 2 h in air by applying 3% water humidified hydrogen as the fuel and ambient air as the cathode

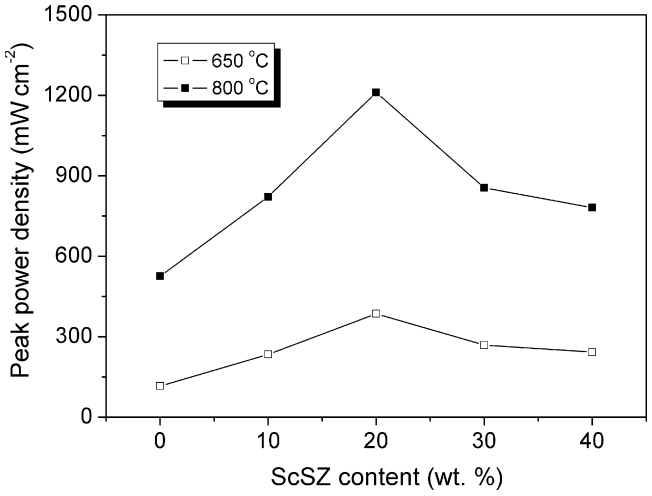

Fig. 11. The peak power densities of single anode-supported cell using various ScSZ contained cathodes at 800 and 650 °C.

atmosphere. It shows that the fuel cell with 80 wt.% LSSM + 20 wt.% ScSZ composite electrodes displayed the best cell performance, in accordance with the results from the three-electrode EIS and step current polarization experiments. For a pure LSSM electrode, a peak power density of 526 mW cm^{-2} was achieved at 800 °C, while it increased to ~1200 mW cm^{-2} when an 80 wt.% LSSM + 20 wt.% ScSZ composite was adopted as the cathode, with greater than 100% improvement. Fig. 12 shows the *I–V* and *I–P* curves of a cell with 80 wt.% LSSM + 20 wt.% ScSZ cathode at various temperatures. A peak power density as high as 386 mW cm^{-2} was still achieved at 650 °C. All the above results support the idea of an 80 wt.% LSSM + 20 wt.% ScSZ composite as a potential cathode for SOFC on ScSZ electrolyte operating at intermediate temperatures.

4. Conclusions

The ionic conductor ScSZ was introduced as a second phase to LSSM perovskite forming a composite electrode for ScSZ-electrolyte solid-oxide fuel cell, which effectively improved the cathodic performance at intermediate temperature. The optimal ScSZ amount is around 20 wt.%; it shows a polarization resistance of ~0.57 Ω cm^2 at 800 °C as compared to a value of ~2.1 Ω cm^2 for a pure LSSM electrode before polarization. The rate-determining step of the oxygen reduction reaction on the composite cathode changed steadily from mainly a surface diffusion process to an electron transfer process with the increase of ScSZ content. A solid-phase reaction between LSSM and ScSZ occurred at 1150 °C or higher, with the formation of a $La_2Zr_2O_7$ insulating phase; however, it did not have a significant impact on the electrode performance. The optimal sintering temperature of the composite cathode with 20 wt.% ScSZ was found to be 1100–1150 °C. Under such sintering temperatures, a favorable connection between LSSM and ScSZ in the electrode was achieved and a high electrode surface area could also be sustained. An anode-supported single cell with a LSSM-20 wt.% ScSZ composite cathode shows promising power densities of ~1211 and 386 mW cm^{-2} at 800 and 650 °C, respectively. Together these results suggest that the LSSM + ScSZ composite electrode is very promising for intermediate-temperature solid-oxide fuel cell application.

Acknowledgements

This work was supported by the National Natural Science Foundation of China under contract nos. 20646002 and 20676061, by National 863 program under contract no. 2007AA05Z133, and

by National Basic Research Program of China under contract no. 2007CB209704. Dr Zongping Shao also would like to acknowledge the financial support from Chinese Ministry of Education via the Program for Changjiang Scholars and Innovative Research Team in University (no. IRT0732).

References

[1] N.Q. Minh, J. Am. Ceram. Soc. 76 (1993) 563–588.
[2] B.C.H. Steele, A. Heinzel, Nature 414 (2001) 345–352.
[3] B.C.H. Steele, Solid State Ionics 86–88 (1996) 1223–1234.
[4] T. Hibino, A. Hashimoto, T. Inoue, J. Tokuno, S. Yoshida, M. Sano, Science 288 (2000) 2031–2033.
[5] Z.P. Shao, S.M. Haile, Nature 431 (2004) 170–173.
[6] T. Hibino, A. Hashimoto, M. Suzuki, M. Sano, J. Electrochem. Soc. 149 (2002) A1503–A1508.
[7] M. Mogensen, K.V. Jensen, M.J. Jørgensen, S. Primdahl, Solid State Ionics 150 (2002) 123–129.
[8] S.B. Adler, Chem. Rev. 104 (2004) 4791–4843.
[9] S.B. Adler, X.Y. Chen, J.R. Wilson, J. Catal. 245 (2007) 91–109.
[10] B.C.H. Steele, Solis State Ionics 94 (1997) 239–248.
[11] Y.H. Lim, J. Lee, J.S. Yoon, C.E. Kim, H.J. Hwang, J. Power Sources 171 (2007) 79–85.
[12] Z. Duan, M. Yang, A. Yan, Z. Hou, Y. Dong, Y. Chong, M. Cheng, W. Yang, J. Power Sources 160 (2006) 57–64.
[13] F.S. Baumann, J. Fleig, H.U. Habermeier, J. Maier, Solid State Ionics 177 (2006) 3187–3191.
[14] J.W. Fergus, J. Power Sources 162 (2006) 30–40.
[15] S. Sarat, N. Sammes, A. Smirnova, J. Power Sources 160 (2006) 892–896.
[16] C. Haering, A. Roosen, H. Schichl, M. Schnoller, Solid State Ionics 176 (2005) 261–268.
[17] O. Yamamoto, Y. Arati, Y. Takeda, N. Imanishi, Y. Mizutani, M. Kawai, Y. Nakamura, Solid State Ionics 124 (1995) 137–142.
[18] V. Brichzin, J. Fleig, H.U. Habermeier, G. Cristiani, J. Maier, Solid State Ionics 152–153 (2002) 499–507.
[19] T. Horita, K. Yamaji, N. Sakai, H. Yokokawa, T. Kawada, T. Kato, Solid State Ionics 127 (2000) 55–65.
[20] T. Horita, K. Yamaji, M. Ishikawa, N. Sakai, H. Yokokawa, T. Kawada, T. Kato, J. Electrochem. Soc. 145 (1998) 3196–3202.
[21] T.Z. Sholklapper, V. Radmilovic, C.P. Jacobson, S.J. Visco, L.C. De Jonghe, J. Power Sources 175 (2008) 206–210.
[22] H. Uchida, M. Yoshida, M. Watanabe, J. Electrochem. Soc. 146 (1999) 1–7.
[23] Y. Huang, K. Huang, F. Luo, L. He, Z. Wang, C. Liao, C. Yana, J. Solid State Chem. 174 (2003) 257–263.
[24] M. Watanabe, H. Uchida, M. Shibata, N. Mochizuki, K. Amikura, J. Electrochem. Soc. 141 (1994) 342–346.
[25] S.P. Jiang, W. Wang, J. Electrochem. Soc. 152 (2005) A1398–A1408.
[26] E.P. Murray, S.A. Barnett, Solid State Ionics 143 (2001) 265–273.
[27] W. Wang, S.P. Jiang, Solis State Ionics 177 (2006) 1361–1369.
[28] Y. Jiang, S. Wang, Y. Zhang, J. Yan, W. Li, J. Electrochem. Soc. 145 (1998) 373–378.
[29] H.Y. Lee, W.S. Cho, S.M. Oh, H.D. Wiemhöfer, W. Göpel, J. Electrochem. Soc. 142 (1995) 2659–2664.
[30] M.J. Jørgensen, M. Mogensen, J. Electrochem. Soc. 148 (2001) A433–A442.
[31] A.C. Co, V.I. Birss, J. Phys. Chem. B. 110 (2006) 11299–11309.
[32] J. Kim, G. Kim, J. Moon, Y. Park, W. Lee, K. Kobayashi, M. Nagai, C. Kim, Solid State Ionics 143 (2001) 379–389.
[33] E. Siebert, A. Hammouche, M. Kleitz, Electrochim. Acta 40 (1995) 1741–1753.
[34] A. Barbucci, M. Viviani, P. Carpanese, D. Vladikova, Z. Stoynoc, Electrochim. Acta 51 (2006) 1641–1650.
[35] M.J. Jørgensen, S. Primdahl, M. Mogensen, Electrochim. Acta 44 (1999) 4195–4201.
[36] S.Z. Wang, Y. Jiang, Y.H. Zhang, J.W. Yan, W.Z. Li, Solid State Ionics 113–115 (1998) 291–303.
[37] T. Suzuki, M. Awano, P. Jasinski, V. Petrovsky, H.U. Anderson, Solid State Ionics 177 (2006) 2071–2074.
[38] E.P. Murray, T. Tsai, S.A. Barnett, Solid State Ionics 110 (1998) 235–243.
[39] S.P. Jiang, J.G. Love, Y. Ramprakash, J. Power Sources 110 (2002) 201–208.
[40] H.X. Gu, Y. Zheng, R. Ran, Z.P. Shao, W.Q. Jin, N.P. Xu, J. Ahn, J. Power Sources 183 (2008) 471–478.
[41] W. Zhou, Z.P. Shao, W.Q. Jin, J. Alloy Compd. 426 (2006) 368–374.
[42] A. Mitterdorfer, L.J. Gauckler, Solid State Ionics 111 (1998) 185–218.
[43] M.J. Escudero, A. Aguadero, J.A. Alonso, L. Daza, J. Electroanal. Chem. 611 (2007) 107–116.
[44] J. Fleig, R. Merkle, J. Maier, Phys. Chem. Chem. Phys. 9 (2007) 2713–2723.
[45] W. Zhou, R. Ran, Z. Shao, W. Zhuang, J. Jia, H. Gu, W. Jin, N. Xu, Acta. Mater. 56 (2008) 2687–2698.
[46] J. Fleig, Annu. Rev. Mater. Res. 33 (2003) 361–382.
[47] F.W. Poulsen, Solid State Ionics 129 (2000) 145–162.
[48] D.S. Mebane, Y. Liu, M. Liu, Solid State Ionics 178 (2008) 1950–1957.